# RF-Search: Searching Unconscious Victim in Smoke Scenes with RF-enabled Drone

Bin-Bin Zhang, Dongheng Zhang, Ruiyuan Song, Binquan Wang, Yang Hu, Yan Chen*
School of Cyber Science and Technology, University of Science and Technology of China
Research Center from Data to Cyberspace, University of Science and Technology of China
Key Lab of Cyberspace Cultural Content Cognition, Communication and Detection, Ministry of Culture and Tourism

## ABSTRACT

Toxic gases inhalation is the most common cause of death in fire scenes, which can make people unconscious and unable to save themselves. Hence, discovering the unconscious victims is crucial to improve their survival rate. In this paper, we propose RF-Search, a victim searching system with RF device mounted on the drone. The challenge mainly comes from the fact that drone motion would overwhelm the subtle vital signs utilized for victim identification. To resolve this problem, we have noted that the physical signature of drone motion has been encoded in stationary object reflections. Leveraging this unique physical signature, we propose to identify the unconscious victim through the spatio-temporal correlation between signals reflected from the victim and the surrounding stationary objects. To extract respiration information of the victim, we propose a motion segmentation module and a motion compensation module to suppress the signal variation caused by drone movement. Extensive experiments have demonstrated that our system could achieve an accuracy of 92.5% for victim identification.

## CCS CONCEPTS

• **Human-centered computing → Ubiquitous and mobile computing systems and tools**.

## KEYWORDS

RF Sensing, Victim Rescue, mmWave Radar

*Corresponding author: Yan Chen (eecyan@ustc.edu.cn).


*ACM MobiCom '23, October 2–6, 2023, Madrid, Spain*

ACM ISBN 978-1-4503-9990-6/23/10…$15.00
https://doi.org/10.1145/3570361.3613305

**ACM Reference Format:**
B. Zhang, D. Zhang, R. Song, B. Wang, Y. Hu, Y. Chen. 2023. RF-Search: Searching Unconscious Victim in Smoke Scenes with RF-enabled Drone. In *The 29th Annual International Conference on Mobile Computing and Networking (ACM MobiCom '23), October 2–6, 2023, Madrid, Spain.* ACM, New York, NY, USA, 15 pages. https://doi.org/10.1145/3570361.3613305

## 1 INTRODUCTION

According to the International Association of Fire and Rescue Services World Fire Statistics, thousands of people die in house fires every year [12], where most fatalities are not due to burns, but a result of inhalation of toxic gases produced during combustion [4, 39]. People soon slip into comas when they inhale toxic gases during fires, which causes unnecessary casualties due to lack of timely discovery and treatment [3, 19]. Therefore, finding the unconscious victim in smoke scenes timely is very critical for rescue. Traditionally, such a mission is completed by the firefighters. However, the high temperature, toxic gases, chaotic and burnt debris, make firefighters in dangerous situations when searching for the victims. Thus, there is an urgent need for the development of mechanical searching systems.

The drone-based search and rescue systems have been widely used due to the maneuverability and flexibility [29, 30, 37]. Equipped with visual cameras [24, 36, 41, 45] and LiDAR [31, 65], these systems can achieve promising performance in ordinary scenarios. However, they cannot be applied in fire scene due to the dense smoke produced by the fire. Recent advancement in the millimeter wave (mmWave) radar makes it a popular sensor in many sensing applications. The mmWave has some very nice and unique characteristics, such as it is non-intrusive and could work under the dense smoke and high temperature conditions. It is thus a natural idea to empower the drone-based search and rescue systems with the mmWave sensing capability.

However, building such as a system is non-trivial. The main challenge is to identify human reflections in the dense smoke scene. Specifically, the reflections from stationary objects in the environment tend to be much stronger than human reflections, which makes it challenging to detect human from raw radar echoes. It has been noted that human respiration would affect the propagation of mmWave signal

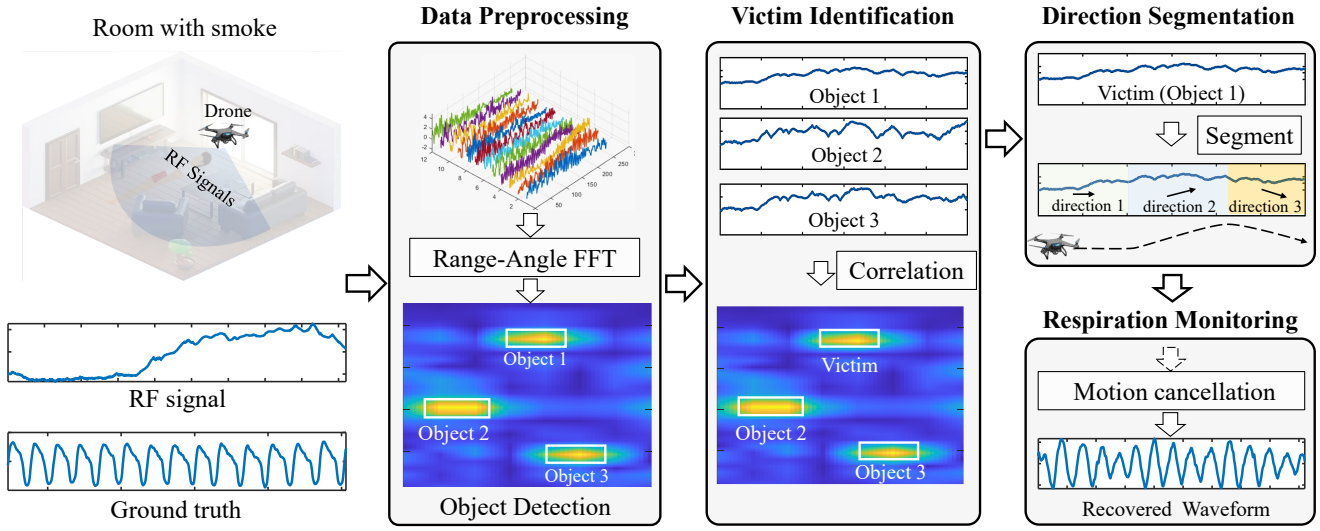


**Figure 1: The proposed RF-Search consists of four components: data preprocessing, victim identification, segmentation of motion direction, and respiratory monitoring. RF-Search first processes the raw signals to generate the range-angle-time representation, then identifies the victim from multiple stationary objects based on the Pearson coefficient. After that, RF-Search segments the drone moving process into multiple time intervals where the motion direction remains unchanged in each interval. Finally, to cancel out the effect of drone motion, RF-Search estimates the compensation coefficient by utilizing a new motion compensation method.**

and make it vary over time, while the reflections from stationary objects keep time-invariant as shown in Figure 2. Such phenomenon has been widely utilized by existing rescue radar systems. However, in our case, this phenomenon no longer holds due to the motion of the radar itself introduced by the drone. What is worse, the respiratory micro-motion would be overwhelmed by the intense and complex drone motion as shown in Figure 3, which makes it difficult to distinguish the victim from stationary objects.

To resolve this challenge, we observe that the time variation of echoes from stationary objects are only determined by the motion of the drone. In other words, the physical signature of drone motion has been encoded in stationary object reflection. As a result, the echoes from different stationary objects are highly correlated even when they are spatially separated. By contrast, the motion caused by human respiration can also modulate the echoes, which destroys the drone motion signature and degrades the correlation of reflections among human and stationary objects. This observation motivates us to identify human reflections by leveraging the signature of drone motion encoded in stationary object reflection.

In this paper, we introduce a novel RF-based drone search and rescue system, RF-Search, which is capable of finding the unconscious victims and monitoring the respiration in complex smoke scene. RF-Search consists of four core components: *Data preprocessing*, *Victim identification*, *Segmentation of drone motion direction*, and *Respiration monitoring*.

First of all, we propose an algorithm to distinguish the unconscious victim from multiple stationary objects. By calculating the Pearson coefficients of the echoes from all detected objects, we take the object with the smallest coefficient value as the unconscious victim. Secondly, we propose to segment the drone motion into multiple time intervals based on the linear relationship of the echoes from the stationary objects. Within each time interval, the drone moves in a constant direction, which would facilitate the monitoring of the respiration. Finally, we recover the respiratory waveform of the victim by cancelling out the drone motion with the proposed motion compensation method. We transform the echoes from the unconscious victim and a stationary object into the frequency domain, then select the frequency band with the highest similarity of energy distribution. The compensation coefficient is estimated by computing the average energy ratio of the two transformed signals in the selected frequency band.

The main contributions of this paper are summarized as follows:

- This paper introduces RF-Search, the first framework which is capable of identifying unconscious victims in smoke scenes with a RF-enabled drone. Leveraging the all-weather nature of mmWave radar and the mobility of the drone,

RF-Search can achieve effective victim identification even under dense smoke condition.

- This paper presents an architecture for victim searching including victim identification, motion segmentation and respiration monitoring, which can identify human reflections effectively and monitor the respiration even under the radar interference introduced by the motion of the drone.
- We implement RF-Search using commodity mmWave radar and drone to evaluate the system performance. Extensive experiments demonstrate that RF-Search could achieve an accuracy of 92.5% for victim identification.

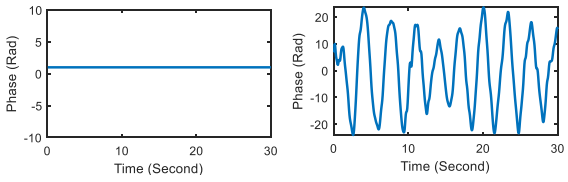


**(a) Stationary object.** **(b) Human respiration.**

**Figure 2: The phase of signals when RF device is static.**

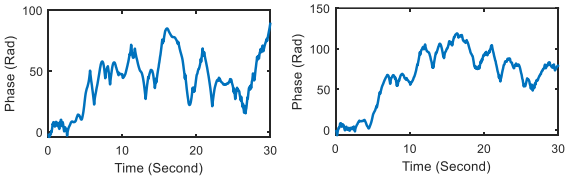


**(a) Stationary object.** **(b) Human respiration.**

**Figure 3: The phase of signals when RF device moves.**

# 2 PRELIMINARY

## 2.1 mmWave signal

We adopt a Frequency Modulated Continuous-Wave (FMCW) radar for signal acquisition. The starting frequency of the radar chirp is $f_c$, and the bandwidth is $B$. The radar will capture the reflected signal, compare it to the original one by mixing them, and then generate the intermediate frequency (IF) signal which can be expressed as:

$$y(t) = A \cdot e^{-j \cdot 2\pi \cdot f_c \cdot \tau}, \tag{1}$$

where $\tau = \frac{2d}{c}$ denotes the delay of signal propagation, $d$ represents the distance between an object and the radar, $c$ is the signal propagation speed in the air, and $A$ denotes the amplitude of the received signal.

After conducting the 2D FFT on the IF signal $y(t)$, we can obtain a three-dimensional matrix representation[1]. The resolution of the range is related to the bandwidth $B$ of the chirp, which can be represented as:

$$d_{res} = \frac{c}{2B}. \tag{2}$$

When $B = 4$ GHz, the resolution of the range is 0.375cm, which means we can locate the position of an object in centimeter level. For finer-grained movement sensing, we need to capture the phase change of the mmWave signals, whose relation with the movement is:

$$\Delta\phi = 2\pi \cdot \frac{2\Delta d}{c} = \frac{4\pi \cdot \Delta d}{c}, \tag{3}$$

where $\Delta d$ denotes the related movement, and $\Delta\phi$ is the phase changes caused by the movement.

## 2.2 Sensing model

When the unconscious victim breathes, there is a micro-motion on the chest. Moreover, the movement of the drone can also result in a change in the distance between the radar and the target. Considering the influence of the respiratory micro-motion and the drone motion on signal propagation, the reflected signal can be represented as:

$$y(t) = A \cdot e^{-j \cdot 2\pi \cdot f_c \cdot (\Delta\tau_{dmov}(t) + \Delta\tau_{rmov}(t) + \tau_{ini})}, \tag{4}$$

where $\Delta\tau_{rmov}(t)$ denotes the delay caused by the respiratory micro-motion, $\Delta\tau_{dmov}(t)$ is the delay caused by the drone motion, and $\tau_{ini}$ is initial delay related to the distance between the victim and the radar. From this sensing model, we can see that both the drone movement and the respiratory movement would affect the signal propagation.

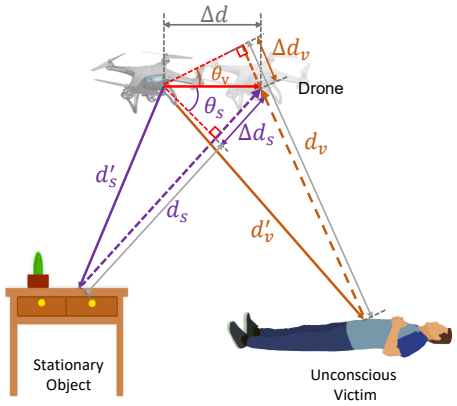


**Figure 4: The signal model of drone motion.**

## 2.3 Drone motion model

The drone moves continuously in the space. As shown in Figure 4, when drone moves by $\Delta d$ in a certain direction, the signal transmission distance changes of a stationary object and the victim are $\Delta d_s$ and $\Delta d_v$ respectively, and the corresponding angles between the direction of the drone motion

[1]The details about the 2D FFT will be described in Section 3.1.

and the direction of signal propagation are $\theta_s$ and $\theta_v$. The relation between $\Delta d_s$ and $\Delta d_v$ can be obtained by

$$\Delta d_v = \Delta d \cdot sin\theta_v = \frac{\Delta d_s}{sin\theta_s} \cdot sin\theta_v = \frac{sin\theta_v}{sin\theta_s} \cdot \Delta d_s = \eta \cdot \Delta d_s, \quad (5)$$

where $\eta = \frac{sin\theta_v}{sin\theta_s}$ is the linear coefficient between $\Delta d_s$ and $\Delta d_v$.

From the above equation, we can see that although the displacements caused by the drone motion on different objects are different, they exhibit a linear correlation relationship during a short time period when the drone keeps a consistent moving direction. Moreover, due to the stochastic nature of the drone's motion, there is a possibility of the angle $\theta_s$ being zero. We therefore add a small constant $\epsilon$ to the denominator and let:

$$\eta = \frac{sin\theta_v}{sin\theta_s + \epsilon}, \quad (6)$$

where $\epsilon = 10^{-12}$. It is worth noting that the respiratory micro-motion of the victim is overwhelmed by the drone motion, which makes it difficult to find the victims and monitor their respiration status. Thus, two key problems of our system are how to distinguish unconscious victims from other detected objects and how to eliminate the influence of drone motion on respiratory sensing.

# 3 RF-SEARCH

The workflow of the proposed system is shown in Figure 1, which mainly consists of four components as follows.

- **Data Preprocessing**: Given the raw input from the radar device, RF-Search first conducts the range FFT and angle FFT transforms to obtain a 3D (range-angle-time) representation.
- **Victim Identification**: The respiratory micro-motion is overwhelmed by the drone motion. It is difficult to distinguish which detected object contains the micro-motion by only using the temporal information. Motivated by the observation that the echo from the stationary object is only modulated by the drone motion while the echo from the victim is modulated by both the drone motion and the respiratory micro-motion, we propose to utilize the Pearson coefficient to exploit the spatial-temporal correlations between the detected objects to identify the victim.
- **Segmentation of Drone Motion Direction**: The information about the drone changing its motion direction can help us cancel out the effect of the drone motion. Hence, we segment the drone motion direction based on the linear coefficient between the signals of stationary objects.
- **Respiration Monitoring**: To monitor the health status of the unconscious victim, we further recover his respiratory waveform which requires cancelling out the phase change caused by the complex drone motion. We propose an effective motion compensation method by utilizing the distribution of the human respiration signal in frequency domain.

## 3.1 Data preprocessing

We perform 2D FFT on raw intermediate frequency (IF) signals to derive the range and angle maps.

***Range FFT:*** The radar continuously transmits FMCW signals, which are also known as chirps. These signals are subsequently captured by the receiving antennas once they are reflected by objects. The mixer of the radar combines the received chirp with the transmitting chirp to generate an IF signal. The relationship between the frequency change $\Delta f$ of the IF signal and the distance $d$ can be expressed as:

$$\Delta f = S \cdot \tau = \frac{S \cdot 2d}{c} \Rightarrow d = \frac{\Delta f \cdot c}{2S}, \quad (7)$$

where $S$ is the slope of the chirp, $c$ is the speed of the signal and $d$ is the distance between the radar and the object. Thus, the range of the detected object can be computed using FFT.

***Angle FFT:*** The computation of the Angle of Arrival (AoA) involves multiple received signals obtained from different antennas. By analyzing the phase changes between adjacent receiving antennas, the relationship between the phase difference $\Delta\phi$ and the AoA $\theta$ can be derived as [54]:

$$\Delta\phi = \frac{2\pi l sin\theta}{\lambda}, \quad (8)$$

where $l$ is the distance between adjacent receiving antennas and $\lambda$ is the wavelength.

By performing the range FFT and angle FFT on each time stamp of received signal, we can obtain a range-angle-time matrix.

## 3.2 Victim identification

The core of this subsection is to find the victim from all detected objects by leveraging the respiratory micro-motion. We first use the CFAR algorithm [35] to detect all existing targets in the smoke scene, including stationary objects and the unconscious victim, based on the energy of the range-angle-time matrix. However, due to the movement of the drone, the respiratory micro-motion is completely overwhelmed by the movement of the drone. As shown in Figure 5, it is difficult to identify which signal contains subtle chest motion. We observe that the echo from the stationary object is only modulated by the drone motion, and thus the echoes from different stationary objects are highly correlated even when they are spatially separated. On the other hand, the echo from the victim is modulated by both the drone motion and the respiratory micro-motion. In such a case, the correlation between the echo from the victim and those from the

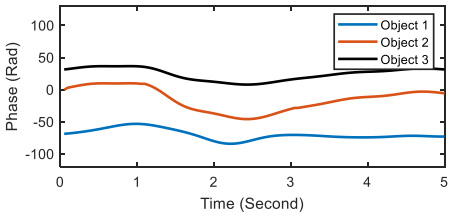


**Figure 5: The echoes of objects. It is difficult to distinguish which one is the victim, because the respiratory micro-motion is overwhelmed by the drone motion.**

stationary objects is weakened. Motivated by this observation, we propose to utilize the strength of the correlations to help identify the victim. Specifically, we use the Pearson coefficient [11] to measure the correlation:

$$\rho_{s1,s2} = \frac{\sum_{i=1}^{n}(P_{s1}^{(i)} - \overline{P}_{s1})(P_{s2}^{(i)} - \overline{P}_{s2})}{\sqrt{\sum_{i=1}^{n}(P_{s1}^{(i)} - \overline{P}_{s1})^2}\sqrt{\sum_{i=1}^{n}(P_{s2}^{(i)} - \overline{P}_{s2})^2 + \epsilon}}, \quad (9)$$

where $P_{s1}, P_{s2}$ denote the phases of signals corresponding to two objects. $\bar{P}_{s1}, \bar{P}_{s2}$ are the average values of $P_{s1}, P_{s2}$. $\rho_{s1,s2}$ denotes the Pearson coefficient between the signals, $n$ is the number of signal samples, $\epsilon = 10^{-12}$. We add a very small constant $\epsilon$ to the denominator to avoid the Pearson coefficient becoming infinite when the denominator is zero.

In Figure 6, we illustrate an example with three detected objects, including two stationary objects and one unconscious victim. According to our previous analysis, since the echoes from the stationary objects are modulated by the same drone motion, the Pearson coefficient between two stationary objects should be close to 1 or -1, as shown in Figure 6c. On the other hand, the Pearson coefficient between a stationary object and the victim should be lower due to the respiratory micro-motion, as shown in Figure 6a and Figure 6b. In such a way, we can identify the victim by finding the object that has low absolute Pearson coefficient with all other objects, e.g., object 1 is identified as the victim in Figure 6.

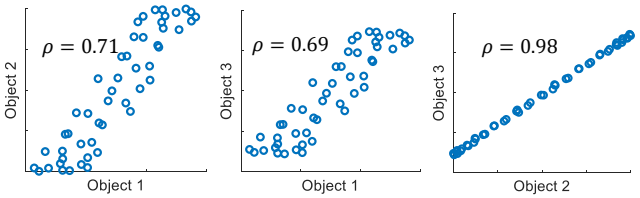


**(a) Object 1-Object 2. (b) Object 1-Object 3. (c) Object 2-Object 3.**

**Figure 6: The Pearson coefficients between pairs of signals. Object 1 is the victim, object 2 and object 3 are stationary objects.**

Furthermore, in scenarios where there are multiple unconscious victims, we can still use the Pearson coefficient to detect them. If the victims are spatially isolated, we identify them sequentially. In scenarios where multiple victims are located in close proximity, the system distinguishes the victims from stationary objects by exploiting the differences between the characteristics of their respiratory patterns, including differences in strength, frequency, and phase. In such a way, the Pearson coefficient between multiple victims would be low, facilitating accurate victim identification.

## 3.3 Segmentation of drone motion direction

After finding the unconscious victim, we intend to further recover his/her respiratory waveform by estimating and eliminating the impact of the drone motion. The drone moves in a relatively fixed direction for a short period of time. The linear relationship between the echoes from two stationary objects effectively reflects the drone motion direction. When the direction of the drone's motion changes, the linear relationship between the echoes from the stationary objects will also change.

Therefore, we propose to segment drone motion direction based on the linear coefficient $\eta_{s1,s2}$ between the echoes from two stationary objects $s1$ and $s2$, which can be calculated by

$$\eta_{s1,s2} = \frac{\sum_{i=1}^{n}(P_{s1}^{(i)} - \bar{P}_{s1})(P_{s2}^{(i)} - \bar{P}_{s2})}{\sum_{i=1}^{n}(P_{s1}^{(i)} - \bar{P}_{s1})^2 + \epsilon}, \quad (10)$$

where $P_{s1}, P_{s2}$ denote the phase of two stationary objects' signals, $\bar{P}_{s1}$ is the average value of $P_{s1}$, and $\bar{P}_{s2}$ is the average value of $P_{s2}$. Moreover, to avoid the denominator being zero, we add a small constant $\epsilon$ to the denominator, where $\epsilon = 10^{-12}$. As shown in Figure 7, we can estimate the coefficient $\eta_{s1,s2}$ between stationary objects within a sliding window, and then use the value of $\eta_{s1,s2}$ to speculate whether the direction of the drone changes or not at each moment.

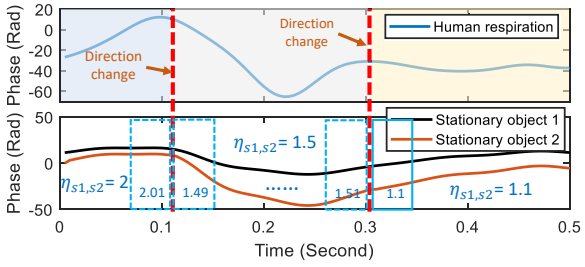


**Figure 7: The drone motion direction is segmented based on whether the value of $\eta_{s1,s2}$ changes. The displacement of the drone within this extremely short duration is minimal due to frequent changes in the drone's direction and its slow speed, which has no effect on the linear coefficient.**

### 3.4 Respiration monitoring

To further understand the health status of the victim, RF-Search recovers the detailed respiratory waveform by estimating and cancelling out the drone motion. Even though the range-angle FFT contains the angle information of the detected object, we cannot directly use it to estimate the motion of drone due to its limited angular and distance resolution. In this work, we indirectly estimate the motion of the drone with the help of stationary objects. The phase change $P_h$ of the signal reflected from a victim consists of two parts: the displacement $P_r$ caused by the respiratory micro-motion and the displacement $P_v$ caused by the drone motion as follow:

$$P_h = P_r + P_v. \tag{11}$$

Since $P_v = \eta_0 \cdot P_s$, where $P_s$ is the phase change of the signal reflected from a stationary object, $\eta_0$ is the ground truth of the linear coefficient, which is adopted as compensation coefficient to estimate the drone motion. In order to eliminate $P_v$, it is necessary to obtain compensation coefficient $\eta_0$. In the literature [58], the least square algorithm [23] has been used to estimate $\eta_0$ by optimizing the following function:

$$\arg\min_{\eta,\xi} \sum_{i=1}^{n} \left(P_h^{(i)} - \left(\eta P_s^{(i)} + \xi\right)\right)^2, \tag{12}$$

where $n$ is the total number of the phase samples, and $\xi$ is a constant. Suppose that $P_h$ is equal to $P_r + \eta_0 P_s$. We can obtain the following results by solving the optimization problem[2]

$$\eta = \eta_0 + \boxed{\frac{\sum_{i=1}^{n}\left(P_s^{(i)} - \bar{P}_s\right)\left(P_r^{(i)} - \bar{P}_r\right)}{\sum_{i=1}^{n}\left(P_s^{(i)} - \bar{P}_s\right)^2}}, \tag{13}$$

where the estimated $\eta$ consists of the ground truth $\eta_0$ and an extra term inside the box. The extra term comes from the influence of micro-motion caused by human respiration. As the extra term cannot be ignored, the drone motion cannot be eliminated by using the estimated $\eta$ from the least square method.

To handle this problem, we propose a novel compensation coefficient estimation method by leveraging the fact that *the frequency band corresponding to the respiratory micro-motion is narrow, while the motion of drone is relatively wide-band.* We first transform the two phases reflected by the stationary object and the victim into the frequency domain and calculate the amplitude of each frequency point as follow:

$$A_s = |FFT(P_s)|, \quad A_h = |FFT(P_h)|, \tag{14}$$

where $FFT$ represents the Fourier transform. $A_s$, $A_h$ are the amplitude of $FFT(P_s)$ and $FFT(P_h)$, respectively. As shown in Figure 8, the frequency distribution is different in respiration band, but similar in other bands.

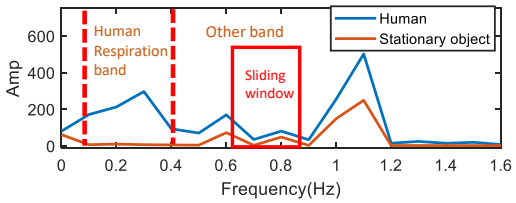


**Figure 8: We transform the echoes from the stationary object and the victim into the frequency domain, then select the frequency band with the highest similarity of energy distribution and compute the energy ratio.**

Then, we design a similarity-based sliding window to identify the non-respiration frequency bands. We calculate the similarity of the frequency amplitude vector in each sliding window and select the sliding window with the highest similarity as follow:

$$\arg\max_{m} \frac{A_s^m \cdot A_h^m}{|A_s^m| \cdot |A_h^m|}, \tag{15}$$

where $A^m$ is the frequency amplitude vector in the $m$-th sliding window, $|\cdot|$ denotes the L1-norm. The ratio between the frequency amplitude with the highest similarity can be calculated as:

$$\eta = \frac{|A_h^m|}{|A_s^m|}, \tag{16}$$

where the ratio $\eta$ is the desired compensation coefficient. It is noticed that we use the L1-norm to calculate the accumulation of energy in this sliding window.

The estimated $\eta$ is adopted to cancel out the drone motion according to the drone motion model. Specifically, we multiply the phase of $y_s(t)$ from the stationary object by the compensation coefficient $\eta$ to obtain $y_s'(t)$ as below:

$$y_s'(t) = A_s \cdot e^{-j\cdot 2\pi \cdot f_c \cdot (\eta \cdot \Delta\tau_{dmov}(t) + \eta \cdot \tau_{ini,s})}. \tag{17}$$

Then, through dividing $y_h(t)$ by $y_s'(t)$, we can eliminate $e^{-j\cdot 2\pi \cdot f_c \Delta\tau_{dmov}(t)}$ caused by the drone motion as follows:

$$y_{new}(t) = \frac{y_h(t)}{y_s'(t)} = \frac{A_h \cdot e^{-j\cdot 2\pi \cdot f_c \cdot \left(\boxed{\Delta\tau_{dmov}(t)} + \Delta\tau_{rmov}(t) + \tau_{ini}\right)}}{A_s \cdot e^{-j\cdot 2\pi \cdot f_c \cdot \left(\boxed{\eta \cdot \Delta\tau_{dmov}(t)} + \eta \cdot \tau_{ini,s}\right)}} \tag{18}$$

$$= \frac{A_h}{A_s} \cdot e^{-j\cdot 2\pi \cdot f_c \cdot (\Delta\tau_{rmov}(t) + \tau_{ini} - \eta \cdot \tau_{ini,s})}, \tag{19}$$

where $A_h$ and $A_s$ are the amplitude signals reflected from the victim and a stationary object, and the expressions inside the two boxes are equal which can be cancelled. Note that $\tau_{ini}$ and $\tau_{ini,s}$ are initial time delay related to object position. After that, the respiratory waveform can be recovered.

[2]The optimization process is shown in **Appendix** A.


(a) Hardware implementation. (b) Scenario.

**Figure 9: Illustrations of the experimental setup.**

## 4 IMPLEMENTATION

**Hardware Implementations.** As shown in Figure 9a, the sensing device of RF-Search mainly contains a mmWave radar module and a wireless communication module that are integrated on the same small PCB board. Thus, the hardware of RF-Search is lightweight and portable, which can be easily integrated into existing commercial drone without any side effects. The mmWave radar employs a TI AWR1843AOP chip [18] that is equipped with 3 transmit antennas and 4 receive antennas, and works at 76 – 81 GHz with 4 GHz available bandwidth. The drone is the Da-Jiang Innovations Mavic 3 [17], which can carry a payload of over 800 grams. The flight path and speed of the drone are controlled through a remote controller. The sensing device and the drone are fixed together with a special adhesive tape. The TP-Link TL-WDR7660 WiFi device is used for receiving and transmitting data. We use a Lenovo thinkpad VE13GTSC laptop with Intel Core-i7 processor and 16GB memory to process data and implement the algorithm.

**Software Implementations.** We configure the radar equipment using Ubuntu 20.04, receive data based on Python 3.8 through WiFi connection, and implement the system based on Matlab.

## 5 PERFORMANCE EVALUATION

In this section, we evaluate the system's performance from two aspects: victim identification and respiratory recovery. Specifically, we first conduct a series of experiments to evaluate the overall system performance. Then we investigate the impact of different experimental factors on the system. Finally, we evaluate the system in indoor and outdoor smoke scenarios.

### 5.1 Experimental setup

We evaluate the proposed RF-Search system under three different indoor environments, i.e., laboratory, conference room, and lobby. We recruit 10 volunteers who repeat the experiment three times in each environment, with each trial lasting 3 minutes, resulting in 270 minutes. We have them lie on the ground in different poses, who are surrounded by some tables, chairs or sofa, as shown in Figure 9b. We also use wearable device HKH-11C with a piezoelectric sensor to collect the ground truth of the subjects' respiration. Our experiments have essentially followed our institute's IRB protocol. During the experiments, we manipulate the drone to enter the experimental scenario to search the subject. To ensure the safety of the drone's flight, it is equipped with an obstacle avoidance system and operates at a low speed. Once the subject is detected, the drone will hover over the subject to sense the respiration.

**Performance metric:** We use the accuracy, precision, and recall as the metrics to evaluate the performance of the victim identification. To evaluate the precision of estimating respiration rates, we utilize the relative error, which is calculated by dividing the absolute error by the actual respiration rates. We also measure the similarity between the recovered respiratory waveform and the ground-truth waveform using the cosine similarity.

**Baseline:** For victim identification, to our best knowledge, the proposed system is the first to detect unconscious victim by detecting respiratory micro-movements under the drone motion. *So there is no proper existing baseline to compare with.* For respiratory waveform recovery, we compare the proposed system with Mobi$^2$Sense [58].

### 5.2 Overall performance

In terms of victim identification, as shown in Figure 11a, our system achieves an accuracy of 92.5%, a precision of 96.5%, and a recall of 93.3% on average, which demonstrates the effectiveness of the proposed system. Moreover, to better illustrate the searching process, we have drawn a diagram of an example of a real-time search process with RF-Search, as shown in Figure 10. In the figure, the horizontal axis represents time, while the vertical axis represents phase. Each line represents the phase of the echo, which reflects the change in distance between the object and the radar. At the beginning, the system detects two objects and identifies them as stationary objects. At 48 second, a new object is identified as a victim. Then the system monitors the victim's breath. At 55 second, two objects are found and identified as stationary objects. From the figure, we are able to gain comprehensive insights into the entire process of searching for unconscious victim, which also demonstrates that our system has the capability of real-time searching. With our hardware setting, the system has a latency of approximately 0.2 seconds. On average, it takes 2 minutes to locate one victim.

When a victim is found, the respiratory waveform is then recovered by the proposed system as shown in Figure 12,

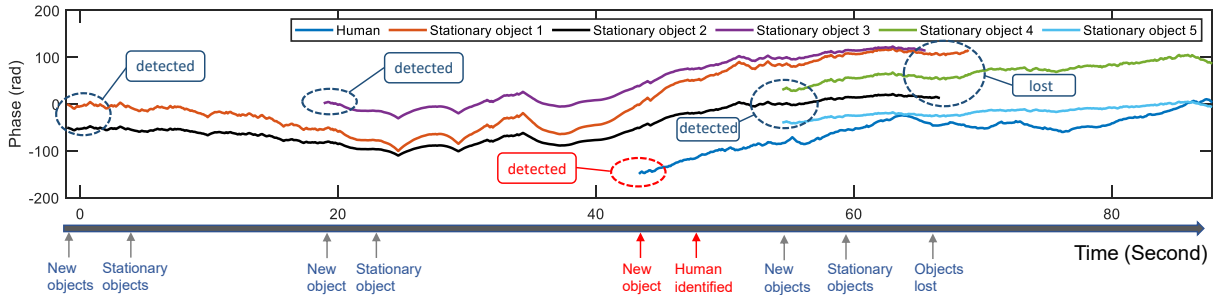


**Figure 10: An example of a real-time search process with the proposed RF-Search. Each line represents the phase of the echo, which reflects the change in distance between the object and the radar. At 48 second, a new object is identified as a victim. Then the system monitors the victim's breath. At about 68 seconds, three objects are lost.**

which has a cosine similarity of 0.91 and respiration rates error of 7% compared with the ground truth. As a comparison, Mobi$^2$Sense [58] only achieves the cosine similarity of 0.66 and respiration rates error of 26% as shown in Figure 11b. This is due to the least squares method for estimating motion compensation coefficient in Mobi$^2$Sense. As evidenced in the Section 3.4, the compensation coefficient that is estimated through least square method contains an extra term, which is the influence of the micro-motion caused by human respiration. As the extra term cannot be ignored, the drone motion cannot be eliminated. The above results demonstrate the superior performance of our system in terms of respiratory waveform recovery and respiration rate estimation.

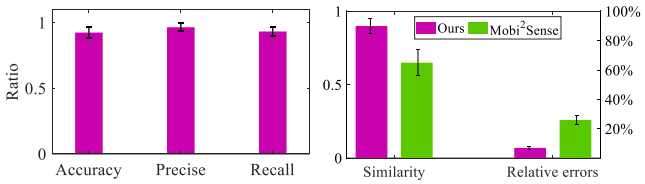


**(a) Victim identification.** **(b) Respiratory recovery.**

**Figure 11: The overall performance of RF-Search.**

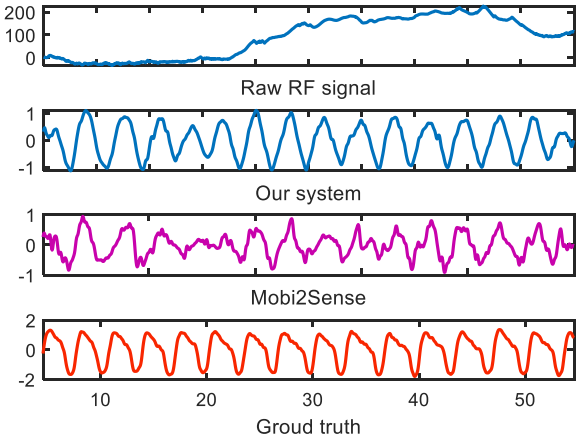


**Figure 12: The recovered respiratory waveform.**

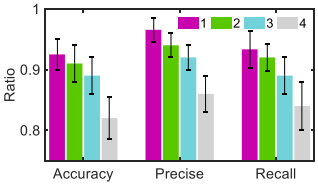


**Figure 13: Impact of number of victims.**

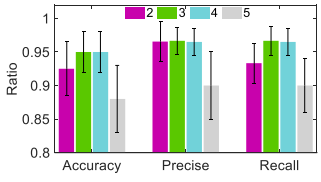


**Figure 14: Impact of number of stationary objects.**

## 5.3 Performance under different scenarios

*5.3.1* ***Impact of multiple unconscious victims.*** In real-world scenarios, RF-Search should be capable of handling situations where multiple victims are located in close proximity and simultaneously scanned by radar. Therefore, we investigate the performance of our system when handling multiple victims. Specifically, we let multiple subjects lie on the ground, who can be simultaneously scanned by radar. And these subjects are separated by about 1 meter apart. We vary the number of subjects from 1 to 4 while keeping other factors unchanged. As shown in Figure 13, our system achieves good identification performance when multiple victims appear simultaneously, where the accuracy is defined by the accuracy of victim identification. Also, with an increasing number of subjects, there is a degradation in identification performance of our system. This is because the respiratory signals of multiple subjects exhibit inherent interferences.

*5.3.2* ***Impact of the number of stationary objects.*** In real-life scenarios, the presence of multiple stationary objects is frequently observed. In this experiment, to study the impact of multiple stationary objects, we change the number

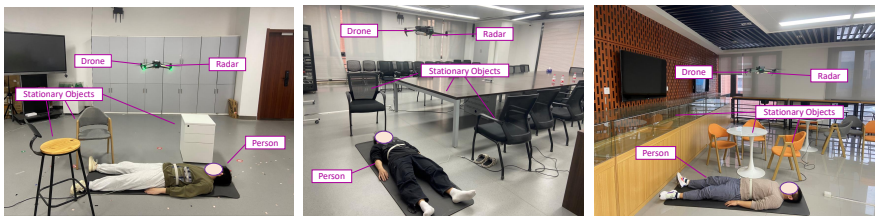


(a) Laboratory. (b) Conference room. (c) Lobby.

**Figure 15: Three different experimental environments.**

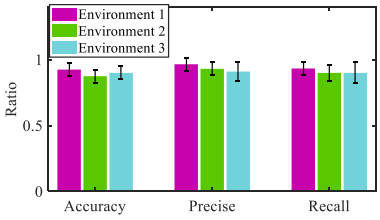


**Figure 16: Impact of environment on victim identification.**

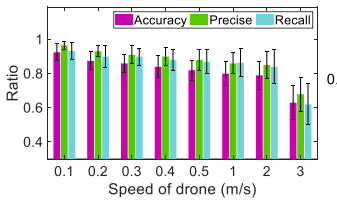


**Figure 17: Impact of the drone's speed.**

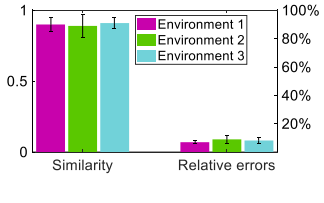


**Figure 18: Impact of environment on respiratory recovery.**

of stationary objects from 2 to 5 while keeping other factors fixed. As show in Figure 14, our system achieves very good performance when the number of stationary objects is 3 and 4, while the performance drops slightly when the number of stationary objects is 2 and 5. This is because too few stationary objects are not conducive enough to remove the drone motion and identify the victim, while too many stationary objects introduce too much interference due to the limited radar distance resolution.

*5.3.3* ***Impact of different speeds of drone.*** To ensure the safe flight of the drone, we control the speed of the drone to fly within a low-speed range. In this subsection, we explore whether the speed of the drone affects the performance of RF-Search. In the experiments, the drone searches for the subjects at speeds ranging from 0.1 m/s to 3 m/s. Figure 17 shows that a higher drone speed will decrease the performance. This is because the Doppler effect leads to some frequency shift, which has an impact on the estimation of compensation coefficient $\eta$ for RF-Search.

*5.3.4* ***Impact of different environments.*** In this subsection, we conduct the experiments on three different environments, i.e., laboratory (length: 8m, width: 7m, height: 4m), conference room (length: 10m, width: 8m, height: 4m), and lobby (length: 8m, width: 8m, height: 4.5m) as shown in Figure 15, to investigate the the system's adaptability to different environments. As shown in Figure 16 and Figure 18, our system achieves similar impressive performance in victim identification and respiratory waveform recovery in different environments, which demonstrates the robustness of the proposed system under different environments.

*5.3.5* ***Impact of different distances between the drone and the victim.*** During the searching process, the distance between the drone and the victim varies depending on the different environmental conditions. Therefore, in this subsection, we investigate whether the distance would influence the performance of our system. Specifically, we deploy the drone to hover above the victim and maintain varying distances, from 1m to 5m. As shown in Table 1, the distances from 1m to 3m do not affect the performance of the system, while at distances of 4m and 5m, the system's performance experiences slightly degradation due to the low power of the radar, which can be addressed by using high-power radar.

**Table 1: Impact of the distances between the drone and the victim.**

| Distances | Acc | Precise | Recall | Similarity | Errors |
|---|---|---|---|---|---|
| 1m | 0.926 | 0.963 | 0.931 | 0.91 | 7.5% |
| 2m | 0.921 | 0.959 | 0.930 | 0.90 | 7.6% |
| 3m | 0.920 | 0.957 | 0.928 | 0.90 | 7.8% |
| 4m | 0.907 | 0.943 | 0.912 | 0.88 | 8.3% |
| 5m | 0.883 | 0.912 | 0.896 | 0.85 | 10.8% |

*5.3.6* ***Impact of different poses of the victim.*** In real-world scenarios, unconscious victim can be with diverse poses when found lying on the ground. To evaluate the impact of different poses of the victim, we conduct a series of experiments, in which the victim lies on the ground with three different poses: lying flat, lying with legs raised, and side lying, as shown in Figure 19a, 19b and 19c. From Figure 19d and 20, we can see that the proposed RF-Search achieves the highest human identification and breath waveform recovery performance when the victim lies flat, while the performance slightly drops when the victim lies on his side. This is because with the victim's lateral decubitus position, the respiratory chest displacement may not be entirely captured by the RF signal.


(a) Lying flat (b) Lying with legs raised

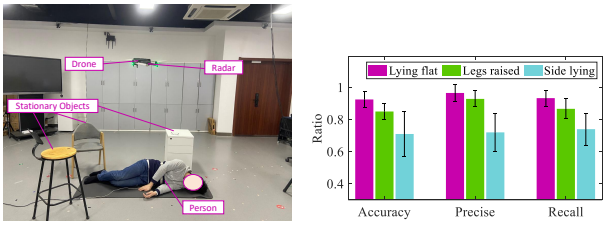


(c) Side lying (d) Results of different poses

**Figure 19: The three poses of victim and the impact of poses on victim search.**

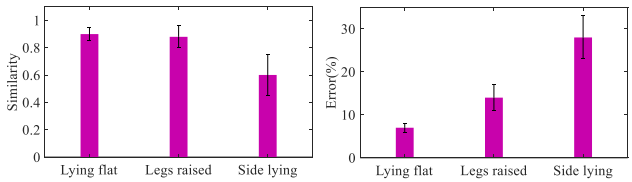


(a) Cosine similarity. (b) Relative errors.

**Figure 20: Impact of poses on respiratory recovery.**

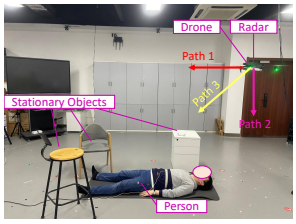


**Figure 21: Three paths.**

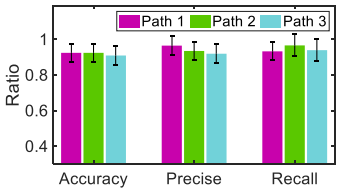


**Figure 22: Impact of paths on victim identification.**

*5.3.7* ***Impact of different flying paths of drone.*** During the operational flights of drone, a wide variety of flight paths are encountered. In this subsection, we investigate the impact of the different drone flying paths on the performance of our system. Specifically, as shown in Figure 21, we control the drone to fly along three different paths. Figure 22 shows that different paths do not affect the performance of our system.

*5.3.8* ***When a person is under a pile of stuffs.*** We also evaluate the performance of the system when a person is under a pile of stuffs. Specifically, the objects with different materials (i.e., cardboard, sponge, wood, metal) are placed on a person lying on the ground. As shown in Table 2, except for the metal, the system still achieves excellent performance when obstructed by other occlusion materials. This is because wireless signals can penetrate through cardboard, sponge, and wood but cannot penetrate metal.

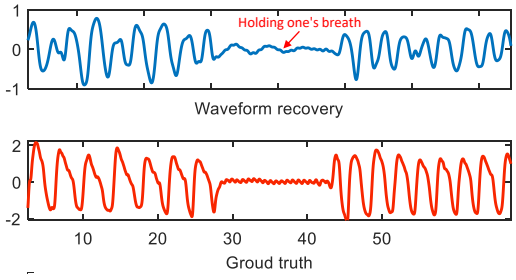


**Figure 23: Detection of abnormal breaths.**

**Table 2: Performance when a person is under stuffs.**

| Material | Acc | Precise | Recall | Similarity | Errors |
|---|---|---|---|---|---|
| Cardboard | 0.915 | 0.952 | 0.921 | 0.90 | 8.6% |
| Sponge | 0.912 | 0.946 | 0.925 | 0.90 | 8.8% |
| Wood | 0.899 | 0.92.6 | 0.912 | 0.89 | 9.2% |
| Metal | 0.501 | 0.582 | 0.517 | 0.53 | 40.6% |

*5.3.9* ***Detection of abnormal respiration.*** Our system can also provide real-time monitoring of the respiratory condition of unconscious victims and promptly transmit health reports. To evaluate the performance of the proposed system on monitoring abnormal breaths, we simulate the abnormal scene by letting the subject holding the breath for a few seconds. Figure 23 shows that our system is able to accurately monitor the abnormal breaths.

## 5.4 Ablation study

*5.4.1* ***Victim identification.*** The CFAR algorithm [35] is adopted to detect all existing targets, which is important for our system. Therefore, we study the impact of the CFAR algorithm on our system. Specifically, we remove the CFAR algorithm, and use the maximum amplitude for target detection. Furthermore, we evaluate the impact of the different window sizes on the CFAR's performance by changing the window size from 4 to 12. As shown in Table 3, the algorithm is essential for our system, and it achieves the best performance when the window size is 8. Moreover, we investigate the impact of the Pearson coefficient, as shown in Figure 24, the blue and red portions represent the Pearson coefficient

between the subject and the stationary objects, and the Pearson coefficient between the stationary objects, respectively. In this work, we set the threshold as 0.87.

**Table 3: The impact of the CFAR algorithm.**

| | W/O | 4 | 6 | 8 | 10 | 12 |
|---|---|---|---|---|---|---|
| Accuracy | 0.769 | 0.836 | 0.916 | **0.925** | 0.920 | 0.856 |
| Precise | 0.778 | 0.854 | 0.957 | **0.965** | 0.959 | 0.879 |
| Recall | 0.756 | 0.841 | 0.926 | **0.933** | 0.928 | 0.863 |

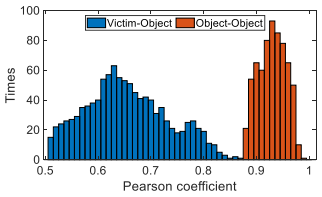


**Figure 24: The distribution of the Pearson coefficient.**

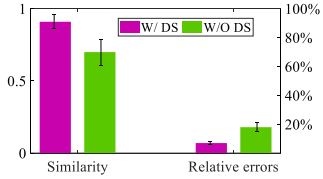


**Figure 25: Impact of Direction Segmentation (DS).**

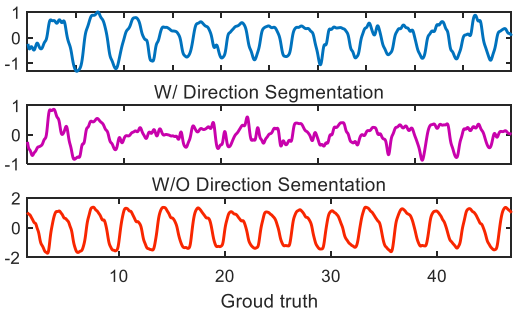


**Figure 26: The impact of motion direction segmentation on respiratory waveform recovery.**

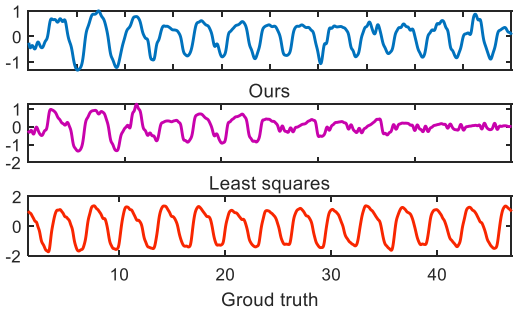


**Figure 27: The impact of different motion compensation methods on respiratory waveform recovery.**

*5.4.2* ***Motion direction segmentation.*** We then evaluate the impact of motion direction segmentation on the performance of our system. Figure 26 illustrates that the similarity between the recovered waveform and the ground truth drops significantly without the motion direction segmentation step. As shown in Figure 25, without motion direction segmentation, the cosine similarity reduces from 0.9 to 0.7, and the breath rate error increases from 7% to 18%. These results demonstrate that the proposed motion direction segmentation is crucial to enable the mmWave radar to sense fine-grained breath under complex drone motion.

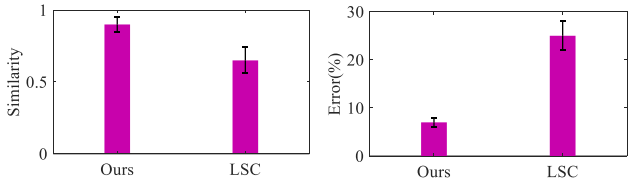


**(a) Cosine similarity.** **(b) Relative errors.**

**Figure 28: Impact of motion compensation methods.**

*5.4.3* ***Motion compensation.*** We also compare the performance of compensation coefficient estimation using the proposed method and the least square method adopted in Mobi$^2$Sense [58]. Figure 27 clearly shows that the recovered waveform by the least square method is worse than our proposed method. Then we compute the cosine similarity between the recovered waveform and ground truth, and the relative error between the estimated and the actual breath rates. As shown in Figure 28, compared with the least square method, our method has achieved significant improvements in both cosine similarity and relative errors.

## 5.5 Case studies

*5.5.1* ***Indoor smoke-filled environment.*** To simulate the smoke-filled scenario, a smoke generator is employed to produce smoke, as shown in Figure 29a. We keep the other experimental settings the same as those under the smoke-free condition. As shown in Table 4, our system has achieved comparable performance to that in a smoke-free scenario. Furthermore, to simulate the scenario of falling burning objects in a fire incident, we allow several objects to fall around the subject. As shown in Figure 31, the distance between the landing area and the victim is approximately 0.5 meters. The results in Table 4 show that the falling objects only have a minimal impact on the performance of the system, where W/ indicates objects falling in the experimental scenario.

*5.5.2* ***Outdoor smoke scenario.*** To simulate the wildfire smoke scenario, we deploy the experiment in an outdoor scenario where a smoke generator is employed to produce

(a) Indoor.

(b) Outdoor.

Figure 29: The two smoke scenarios.


Figure 30: Outdoor scenario setup.

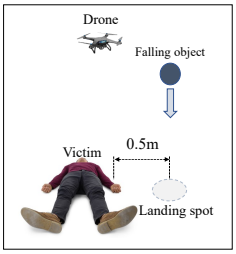


Figure 31: Falling objects scenario.

Table 4: The performance in indoor smoke scenario.

| Falling objects | Acc | Precise | Recall | Similarity | Errors |
|---|---|---|---|---|---|
| W/O | 0.926 | 0.963 | 0.931 | 0.91 | 7.5% |
| W/ | 0.901 | 0.946 | 0.925 | 0.90 | 8.2% |

Table 5: The performance in outdoor smoke scenario.

| Scenario | Acc | Precise | Recall | Similarity | Errors |
|---|---|---|---|---|---|
| Indoor | 0.926 | 0.963 | 0.931 | 0.91 | 7.5% |
| **Outdoor** | 0.881 | 0.926 | 0.896 | 0.83 | 12.7% |

smoke, as shown in Figure 29b. We let the subject lie on an unmanned vacant land, while the drone searching within a certain vicinity. The vertical distance between the drone and the subject ranges from 2 meters to 5 meters. The setup in outdoor experiment is shown in Figure 30. The results in Table 5 show that the system experiences a certain degree of performance degradation compared to indoor scenarios due to fewer stationary objects available as references.

## 6 RELATED WORK

**RF sensing** has recently attracted tremendous attentions in both academia and industry. It has been employed to solve various human-related problems including human gesture recognition [16, 25, 43, 44, 59], activity recognition [8, 13, 20, 46, 49, 50], pose estimation [21, 38, 60, 62], human mesh recovery [51, 52, 61], silhouette generation[38, 48], re-identification [14, 26], fall detection [27, 42], vital sign monitoring [9, 10, 55–57, 63], localization [22, 47, 53] and so on. These existing works mainly rely on static transmitter and receiver deployment which hinders the application of large-scale RF based sensing in practice. In this work, we aims to conduct RF sensing with the sensing device mounted on a drone which moves in a complex way.

**Device mobility** sensing system with RF aims to overcome the effect of signal variation caused by device movement. Airborne radar [40] and vehicular radar [6] are two classic device mobility sensing systems, which are widely used to sense nearby objects' locations and moving speed, but cannot meet the requirements of complex perception tasks [32]. To enable more fine-grained sensing like monitoring the millimeter level respiration movement (rate and depth), Mobi$^2$Sense [58] employs one static object in the environment as a reference to remove the effect of device movement. Although these existing device mobility sensing systems have made much progress in dealing with the device movement, they still are inapplicable to micro-motion identification under complex device motion like drone move and are unable to effectively cancel the influence of the motion. The proposed method can identify stationary targets with micro-motion using RF device with very complex motion pattern.

**Vital sign monitoring** aims to recover the fine-grained vital sign from the subtle micro-motions using RF sensing device, including heartbeat [1, 7, 15, 63] and breath [1, 55, 56, 58, 63]. These micro-motions are extremely sensitive to the body or device movements, and can be easily submerged by high-energy movements. So existing vital sign monitoring only works in limited scenarios, e.g., static target or device. To tackle these challenges, MoRe-Fi [64] and MoVi-Fi [10] extend the above limited scenarios to a relaxed one with body movements and employs customized deep learning approaches for the problem. But the devices are still kept static in these works. Mobi$^2$Sense [58] allows the movement of the device and chooses a static object in the scene as a reference to remove the effect of device move. The device movement considered in our work is much more complex and we further considered the static reference object identification problem. We propose to utilize the spatial-temporal correlation between the sensed objects to effectively identify the unconscious victim and the static reference object.

## 7 LIMITATIONS AND DISCUSSIONS

**Stationary objects and reference:** Our system requires two or more stationary objects as references in order to identify the subject. While such a condition generally holds

in most scenarios, the performance may degrade when there is only one or no stationary object. Moreover, due to the relatively large surface area of walls and floors, the radar reflections from the walls and floors exhibit variations as the drone moves. Thus, the floors and walls cannot be considered as a reference to estimate the drone motion.

**Drone motion:** Although our system is applicable in any motion direction and location of the drone, it assumes that the motion of the drone is translational. However, the actual movement of drones is even more diverse and intricate. In addition to translation, it involves other motions such as rotation. In future work, we will delve deeper into modeling drone movement in order to address the impact of drone motion on system performance.

**Path plannings:** For the path plannings, existing works [2, 5, 28, 33, 34] are relatively mature. In this paper, our focus is on how to search victims and recover the respiratory waveform under drone motion. In future work, we will combine our method with the path planning algorithm to achieve a faster and more intelligent search and rescue system.

**Multi-drone cooperation:** Multi-drone cooperative search can enhance search efficiency, but there can be interference among the radars on the drones due to operating in the same frequency range. In the future, we will integrate the interference mitigation techniques to facilitate multi-drone cooperation.

## 8 CONCLUSION

While radar human detection based on vital signs has been studied for years, the situation where the radar is mounted on the drone has never been explored. To resolve the signal variations raised by drone motion, we have noted that the physical signature of drone motion is encoded in stationary object reflections. Based on this observation, we propose an architecture for victim searching which takes victim identification, motion segmentation and respiration monitoring as the core components. Extensive experiments demonstrate that the proposed framework could achieve an accuracy of 92.5% for victim identification. To the best of our knowledge, this is the first framework which is capable of identifying unconscious victims in smoke scenes with a RF-enabled drone.

## A DETAILED PROOF OF EQUATION

For convenience of presentation, we redefine our problem in a mathematical manner.

Given the phase of the received signal $P_h$, we can divide it into $P_r$ and $P_v$ as:

$$P_h = P_r + P_v \tag{20}$$

where $P_v = \eta_0 \cdot P_s$. So we have $P_h = P_r + \eta_0 \cdot P_s$.

The $\eta_0$ is unknown, and we need to estimate the value of $\eta_0$ from a series of observation value, e.g., $P_s$ and $P_h$. Existing method [58] assumes that $P_r$ is approximately a constant $\xi$, and estimates $\eta_0$ through the least square method by minimizing the following function:

$$F(\eta, \xi) = \sum_{i=1}^{n} \left( P_h^{(i)} - \left( \eta P_s^{(i)} + \xi \right) \right)^2, \tag{21}$$

where $\eta$ is the estimated value of $\eta_0$. The least square method obtains the minimum by setting $\frac{\partial F}{\partial \eta} = 0$, $\frac{\partial F}{\partial \xi} = 0$ as:

$$\frac{\partial F}{\partial \eta} = 2 \sum_{i=1}^{n} \left( P_h^{(i)} - \left( \eta P_s^{(i)} + \xi \right) \right) \left( -P_s^{(i)} \right) = 0, \tag{22}$$

$$\frac{\partial F}{\partial \xi} = 2 \sum_{i=1}^{n} \left( P_h^{(i)} - \left( \eta P_s^{(i)} + \xi \right) \right) (-1) = 0, \tag{23}$$

which gives

$$\xi = \bar{P}_h - \bar{P}_s, \tag{24}$$

$$\eta = \frac{\sum_{i=1}^{n} \left( P_s^{(i)} - \bar{P}_s \right) \left( P_h^{(i)} - \bar{P}_h \right)}{\sum_{i=1}^{n} \left( P_s^{(i)} - \bar{P}_s \right)^2}, \tag{25}$$

where $\bar{P}_h = \frac{1}{n} \sum_{i=1}^{n} P_h^{(i)}$ and $\bar{P}_s = \frac{1}{n} \sum_{i=1}^{n} P_s^{(i)}$. Substituting $P_h = P_r + \eta_0 \cdot P_s$ into above equation, the estimated value $\eta$ is

$$\eta = \frac{\sum_{i=1}^{n} \left( P_s^{(i)} - \bar{P}_s \right) \left( P_r^{(i)} + \eta_0 P_s^{(i)} - \bar{P}_r - \eta_0 \bar{P}_s \right)}{\sum_{i=1}^{n} \left( P_s^{(i)} - \bar{P}_s \right)^2} \tag{26}$$

$$= \eta_0 + \boxed{\frac{\sum_{i=1}^{n} \left( P_s^{(i)} - \bar{P}_s \right) \left( P_r^{(i)} - \bar{P}_r \right)}{\sum_{i=1}^{n} \left( P_s^{(i)} - \bar{P}_s \right)^2}}, \tag{27}$$

which has the same mathematical form with Equation.13.


## ACKNOWLEDGEMENT

We are grateful to the shepherd and the reviewers for their valuable and constructive comments. We would like to thank Yun Wu, Jianwen Tong for providing us hardware support. This work was supported by National Key R&D Programmes under Grant 2022YFC0869800 and 2022YFC2503405, National Natural Science Foundation of China under Grant 62201542 and 62172381, fellowship of China Postdoctoral Science Foundation under grant 2022M723069, and the Fundamental Research Funds for the Central Universities.


## REFERENCES


[1] Fadel Adib, Hongzi Mao, Zachary Kabelac, Dina Katabi, and Robert C. Miller. 2015. Smart Homes That Monitor Breathing and Heart Rate. In *Proc. of the 33rd ACM CHI*. 837–846.

[2] Shubhani Aggarwal, Neeraj Kumar, Musaed Alhussein, and Ghulam Muhammad. 2021. Blockchain-based UAV path planning for healthcare 4.0: Current challenges and the way ahead. *IEEE Network* 35, 1 (2021), 20–29.

[3] AAS Alarifi, Herodotos N Phylaktou, and Gordon E Andrews. 2016. What kills people in a fire? heat or smoke? *9th SSC Proceedings* (2016).

[4] Marc J Assael and Konstantinos E Kakosimos. 2010. *Fires, explosions, and toxic gas dispersions: effects calculation and risk analysis.* CRC Press.

[5] Harald Bayerlein, Mirco Theile, Marco Caccamo, and David Gesbert. 2021. Multi-UAV path planning for wireless data harvesting with deep reinforcement learning. *IEEE Open Journal of the Communications Society* 2 (2021), 1171–1187.

[6] Holger Caesar, Varun Bankiti, Alex H. Lang, Sourabh Vora, Venice Erin Liong, Qiang Xu, Anush Krishnan, Yu Pan, Giancarlo Baldan, and Oscar Beijbom. 2020. nuScenes: A Multimodal Dataset for Autonomous Driving. In *Proc. of the IEEE/CVF CVPR*. 11618–11628.

[7] Jinbo Chen, Dongheng Zhang, Zhi Wu, Fang Zhou, Qibin Sun, and Yan Chen. 2022. Contactless Electrocardiogram Monitoring With Millimeter Wave Radar. *IEEE Transactions on Mobile Computing* (2022), 1–17.

[8] Yan Chen, Hongyu Deng, Dongheng Zhang, and Yang Hu. 2021. SpeedNet: Indoor Speed Estimation With Radio Signals. *IEEE Internet of Things Journal* 8, 4 (2021), 2762–2774.

[9] Yan Chen, Xiang Su, Yang Hu, and Bing Zeng. 2020. Residual Carrier Frequency Offset Estimation and Compensation for Commodity WiFi. *IEEE Transactions on Mobile Computing* 19, 12 (2020), 2891–2902.

[10] Zhe Chen, Tianyue Zheng, Chao Cai, and Jun Luo. 2021. MoVi-Fi: Motion-Robust Vital Signs Waveform Recovery via Deep Interpreted RF Sensing. In *Proc. of the 27th ACM MobiCom (MobiCom '21)*. 392–405.

[11] Israel Cohen, Yiteng Huang, Jingdong Chen, Jacob Benesty, Jacob Benesty, Jingdong Chen, Yiteng Huang, and Israel Cohen. 2009. Pearson correlation coefficient. *Noise reduction in speech processing* (2009), 1–4.

[12] CTIF. 2022. World Fire Statistics. https://www.ctif.world-fire-statistics.

[13] Shuya Ding, Zhe Chen, Tianyue Zheng, and Jun Luo. 2020. RF-Net: A Unified Meta-Learning Framework for RF-Enabled One-Shot Human Activity Recognition. In *Proc. of the 18th ACM SenSys*. 517–530.

[14] Lijie Fan, Tianhong Li, Rongyao Fang, Rumen Hristov, Yuan Yuan, and Dina Katabi. 2020. Learning Longterm Representations for Person Re-Identification Using Radio Signals. In *Proc. of the IEEE/CVF CVPR*. 10696–10706.

[15] Unsoo Ha, Salah Assana, and Fadel Adib. 2020. Contactless Seismocardiography via Deep Learning Radars. In *Proc. of the 26th ACM MobiCom*.

[16] Ying He, Yan Chen, Yang Hu, and Bing Zeng. 2020. WiFi Vision: Sensing, Recognition, and Detection With Commodity MIMO-OFDM WiFi. *IEEE Internet of Things Journal* 7, 9 (2020), 8296–8317.

[17] Da-Jiang Innovations. 2022. Mavic 3. https://www.dji.com/cn/mavic-3/specs.

[18] Texas Instruments. 2020. AWR1843AOP. https://www.ti.com/product/AWR1843AOP?keyMatch=AWR1843AOP. Accessed: 2022-03-03.

[19] Mastura Jaafar, Nuzaihan Aras Agus Salim, Naziah Muhamad Salleh, Mohd Zailan Sulieman, Norhidayah Md Ulang, and Andrew Ebekozien. 2021. Developing a framework for fire safety management plan: the case of Malaysia's public hospital buildings. *International Journal of Building Pathology and Adaptation* ahead-of-print (2021).

[20] Wenjun Jiang, Chenglin Miao, Fenglong Ma, Shuochao Yao, Yaqing Wang, Ye Yuan, Hongfei Xue, Chen Song, Xin Ma, Dimitrios Koutsonikolas, Wenyao Xu, and Lu Su. 2018. Towards Environment Independent Device Free Human Activity Recognition. In *Proc. of the 24th ACM MobiCom*. 289–304.

[21] Wenjun Jiang, Hongfei Xue, Chenglin Miao, Shiyang Wang, Sen Lin, Chong Tian, Srinivasan Murali, Haochen Hu, Zhi Sun, and Lu Su. 2020. Towards 3D Human Pose Construction Using Wifi. In *Proc. of the 26th ACM MobiCom*. Article 23, 14 pages.

[22] Manikanta Kotaru, Kiran Joshi, Dinesh Bharadia, and Sachin Katti. 2015. SpotFi: Decimeter Level Localization Using WiFi. In *Proc. of the ACM SIGCOMM*. 269–282.

[23] Tze Leung Lai, Herbert Robbins, and Ching Zong Wei. 1978. Strong consistency of least squares estimates in multiple regression. *Proceedings of the national academy of sciences* 75, 7 (1978), 3034–3036.

[24] Seoungjun Lee, Dongsoo Har, and Dongsuk Kum. 2016. Drone-assisted disaster management: Finding victims via infrared camera and lidar sensor fusion. In *2016 3rd Asia-Pacific World Congress on Computer Science and Engineering (APWC on CSE)*. IEEE, 84–89.

[25] Hong Li, Wei Yang, Jianxin Wang, Yang Xu, and Liusheng Huang. 2016. WiFinger: Talk to Your Smart Devices with Finger-Grained Gesture. In *Proc. of the ACM UbiComp (UbiComp '16)*. 250–261.

[26] Tianhong Li, Lijie Fan, Yuan Yuan, and Dina Katabi. 2022. Unsupervised Learning for Human Sensing Using Radio Signals. In *Proc. of the IEEE/CVF WACV*. 1091–1100.

[27] Wenxuan Li, Dongheng Zhang, Yadong Li, Zhi Wu, Jinbo Chen, Dong Zhang, Yang Hu, Qibin Sun, and Yan Chen. 2022. Real-Time Fall Detection Using Mmwave Radar. In *Proc. of the IEEE ICASSP*. 16–20.

[28] Yucong Lin and Srikanth Saripalli. 2017. Sampling-based path planning for UAV collision avoidance. *IEEE Transactions on Intelligent Transportation Systems* 18, 11 (2017), 3179–3192.

[29] Eleftherios Lygouras, Nicholas Santavas, Anastasios Taitzoglou, Konstantinos Tarchanidis, Athanasios Mitropoulos, and Antonios Gasteratos. 2019. Unsupervised human detection with an embedded vision system on a fully autonomous UAV for search and rescue operations. *Sensors* 19, 16 (2019), 3542.

[30] Balmukund Mishra, Deepak Garg, Pratik Narang, and Vipul Mishra. 2020. Drone-surveillance for search and rescue in natural disaster. *Computer Communications* 156 (2020), 1–10.

[31] Constantine Papageorgiou and Tomaso Poggio. 2000. A trainable system for object detection. *International journal of computer vision* 38 (2000), 15–33.

[32] Kun Qian, Zhaoyuan He, and Xinyu Zhang. 2020. 3D Point Cloud Generation with Millimeter-Wave Radar. In *Proc. ACM Interact. Mob. Wearable Ubiquitous Technol.*, Vol. 4.

[33] Shankarachary Ragi and Edwin KP Chong. 2013. UAV path planning in a dynamic environment via partially observable Markov decision process. *IEEE Trans. Aerospace Electron. Systems* 49, 4 (2013), 2397–2412.

[34] Vincent Roberge, Mohammed Tarbouchi, and Gilles Labonté. 2012. Comparison of parallel genetic algorithm and particle swarm optimization for real-time UAV path planning. *IEEE Transactions on industrial informatics* 9, 1 (2012), 132–141.

[35] Frank C Robey, Daniel R Fuhrmann, Edward J Kelly, and Ramon Nitzberg. 1992. A CFAR adaptive matched filter detector. *IEEE Transactions on aerospace and electronic systems* 28, 1 (1992), 208–216.

[36] Santiago Royo and Maria Ballesta-Garcia. 2019. An overview of lidar imaging systems for autonomous vehicles. *Applied sciences* 9, 19 (2019), 4093.

[37] David C Schedl, Indrajit Kurmi, and Oliver Bimber. 2021. An autonomous drone for search and rescue in forests using airborne optical sectioning. *Science Robotics* 6, 55 (2021), eabg1188.

[38] Ruiyuan Song, Dongheng Zhang, Zhi Wu, Cong Yu, Chunyang Xie, Shuai Yang, Yang Hu, and Yan Chen. 2022. RF-URL: Unsupervised Representation Learning for RF Sensing. In *Proc. of the 28th ACM MobiCom*. 282–295.

[39] Maria Stefanidou, Sotiris Athanaselis, and Chara Spiliopoulou. 2008. Health impacts of fire smoke inhalation. *Inhalation toxicology* 20, 8 (2008), 761–766.

[40] George W Stimson. 1998. *Introduction to airborne radar*. SciTech Publishing, Inc.

[41] Jarosław Szrek, Radosław Zimroz, Jacek Wodecki, Anna Michalak, Mateusz Góralczyk, and Magdalena Worsa-Kozak. 2020. Application of the infrared thermography and unmanned ground vehicle for rescue action support in underground mine—The amicos project. *Remote Sensing* 13, 1 (2020), 69.

[42] Yonglong Tian, Guang-He Lee, Hao He, Chen-Yu Hsu, and Dina Katabi. 2018. RF-Based Fall Monitoring Using Convolutional Neural Networks. *Proc. ACM Interact. Mob. Wearable Ubiquitous Technol.* 2, 3, Article 137 (sep 2018), 24 pages.

[43] Raghav H. Venkatnarayan, Shakir Mahmood, and Muhammad Shahzad. 2021. WiFi based Multi-User Gesture Recognition. *IEEE Transactions on Mobile Computing* 20, 3 (2021), 1242–1256.

[44] Aditya Virmani and Muhammad Shahzad. 2017. Position and Orientation Agnostic Gesture Recognition Using WiFi. In *Proc. of the 15th ACM MobiSys (MobiSys '17)*. 252–264.

[45] T Thuy Vu, Fumio Yamazaki, and Masashi Matsuoka. 2009. Multi-scale solution for building extraction from LiDAR and image data. *International Journal of Applied Earth Observation and Geoinformation* 11, 4 (2009), 281–289.

[46] Yan Wang, Jian Liu, Yingying Chen, Marco Gruteser, Jie Yang, and Hongbo Liu. 2014. E-Eyes: Device-Free Location-Oriented Activity Identification Using Fine-Grained WiFi Signatures. In *Proc. of the 20th ACM MobiCom (MobiCom '14)*. 617–628.

[47] Chenshu Wu, Feng Zhang, Beibei Wang, and K. J. Ray Liu. 2020. mmTrack: Passive Multi-Person Localization Using Commodity Millimeter Wave Radio. In *Proc. of the IEEE INFOCOM 2020*. 2400–2409.

[48] Zhi Wu, Dongheng Zhang, Chunyang Xie, Cong Yu, Jinbo Chen, Yang Hu, and Yan Chen. 2022. RFMask: A Simple Baseline for Human Silhouette Segmentation With Radio Signals. *IEEE Transactions on Multimedia* (2022), 1–12.

[49] Qinyi Xu, Yan Chen, BeiBei Wang, and K. J. Ray Liu. 2017. Radio Biometrics: Human Recognition Through a Wall. *IEEE Transactions on Information Forensics and Security* 12, 5 (2017), 1141–1155.

[50] Qinyi Xu, Yan Chen, Beibei Wang, and K. J. Ray Liu. 2017. TRIEDS: Wireless Events Detection Through the Wall. *IEEE Internet of Things Journal* 4, 3 (2017), 723–735.

[51] Hongfei Xue, Qiming Cao, Yan Ju, Haochen Hu, Haoyu Wang, Aidong Zhang, and Lu Su. 2021. MmMesh: Towards 3D Real-Time Dynamic Human Mesh Construction Using Millimeter-Wave. In *Proc. of the 20th ACM MobiSys*. 391–406.

[52] Hongfei Xue, Yan Ju, Chenglin Miao, Yijiang Wang, Shiyang Wang, Aidong Zhang, and Lu Su. 2023. M4esh: MmWave-Based 3D Human Mesh Construction for Multiple Subjects. In *Proc. of the 19th ACM SenSys*. 269–282.

[53] Shuai Yang, Dongheng Zhang, Ruiyuan Song, Pengfei Yin, and Yan Chen. 2023. Multiple WiFi Access Points Co-Localization Through Joint AoA Estimation. *IEEE Transactions on Mobile Computing* (2023), 1–16.

[54] Dongheng Zhang, Ying He, Xinyu Gong, Yang Hu, Yan Chen, and Bing Zeng. 2018. Multitarget AOA estimation using wideband LFMCW signal and two receiver antennas. *IEEE Transactions on Vehicular Technology* 67, 8 (2018), 7101–7112.

[55] Dongheng Zhang, Yang Hu, and Yan Chen. 2021. MTrack: Tracking Multiperson Moving Trajectories and Vital Signs With Radio Signals. *IEEE Internet of Things Journal* 8, 5 (2021), 3904–3914.

[56] Dongheng Zhang, Yang Hu, Yan Chen, and Bing Zeng. 2019. BreathTrack: Tracking indoor human breath status via commodity WiFi. *IEEE Internet of Things Journal* 6, 2 (2019), 3899–3911.

[57] Dongheng Zhang, Yang Hu, Yan Chen, and Bing Zeng. 2020. Calibrating Phase Offsets for Commodity WiFi. *IEEE Systems Journal* 14, 1 (2020), 661–664.

[58] Fusang Zhang, Jie Xiong, Zhaoxin Chang, Junqi Ma, and Daqing Zhang. 2022. Mobi2Sense: empowering wireless sensing with mobility. In *Proceedings of the 28th Annual International Conference on Mobile Computing And Networking*. 268–281.

[59] Yi Zhang, Yue Zheng, Kun Qian, Guidong Zhang, Yunhao Liu, Chenshu Wu, and Zheng Yang. 2021. Widar3.0: Zero-Effort Cross-Domain Gesture Recognition with Wi-Fi. *IEEE Transactions on Pattern Analysis and Machine Intelligence* (2021), 1–1.

[60] Mingmin Zhao, Tianhong Li, Mohammad Abu Alsheikh, Yonglong Tian, Hang Zhao, Antonio Torralba, and Dina Katabi. 2018. Through-Wall Human Pose Estimation Using Radio Signals. In *Proc. of the IEEE/CVF CVPR*. 7356–7365.

[61] Mingmin Zhao, Yingcheng Liu, Aniruddh Raghu, Hang Zhao, Tianhong Li, Antonio Torralba, and Dina Katabi. 2019. Through-Wall Human Mesh Recovery Using Radio Signals. In *Proc. of the IEEE/CVF ICCV*. 10112–10121.

[62] Mingmin Zhao, Yonglong Tian, Hang Zhao, Mohammad Abu Alsheikh, Tianhong Li, Rumen Hristov, Zachary Kabelac, Dina Katabi, and Antonio Torralba. 2018. RF-Based 3D Skeletons. In *Proc. of the ACM SIGCOMM (SIGCOMM '18)*. 267–281.

[63] Tianyue Zheng, Zhe Chen, Chao Cai, Jun Luo, and Xu Zhang. 2020. V2iFi: In-Vehicle Vital Sign Monitoring via Compact RF Sensing. In *Proc. ACM Interact. Mob. Wearable Ubiquitous Technol.*

[64] Tianyue Zheng, Zhe Chen, Shujie Zhang, Chao Cai, and Jun Luo. 2021. MoRe-Fi: Motion-Robust and Fine-Grained Respiration Monitoring via Deep-Learning UWB Radar. In *Proc. of the 19th ACM SenSys*. 111–124.

[65] Zhengxia Zou, Keyan Chen, Zhenwei Shi, Yuhong Guo, and Jieping Ye. 2023. Object detection in 20 years: A survey. *Proc. IEEE* (2023).